An assessment of representing land-ocean heterogeneity via convective adjustment timescale in the Community Atmospheric Model 6 (CAM6)

Bidyut Bikash Goswami[1], **Andrea Polesello**[1], **Caroline Muller**[1]

[1]Institute of Science and Technology Austria (ISTA), Klosterneuburg, Austria

Key Points:

- Two distinct values of convective adjustment timescale, τ, over land & ocean in the convective parameterization scheme are prescribed.
- The mean climate stays qualitatively the same, except for a moister and colder near-surface atmosphere for longer τs over the oceans.
- A primary gain of using two different τs for land and ocean is improved simulation of the convectively coupled equatorial waves.

Corresponding author: B. B. Goswami, bgoswami@ista.ac.at

Abstract

The time needed by deep convection to bring the atmosphere back to equilibrium is called convective adjustment timescale or simply adjustment timescale, typically denoted by τ. In the Community Atmospheric Model (CAM), convective adjustment timescale is a tunable parameter with one value, 1 hour, worldwide. Albeit, there is no justified reason why one adjustment timescale value should work over land and ocean both. Continental and oceanic convection are different in terms of the vigor of updrafts and hence can have different longevities. So it is logical to investigate the prescription of two different convective adjustment timescales for land (τ_L) and ocean (τ_O). To understand the impact of representing land-ocean heterogeneity via τ, we investigate CAM climate simulations for two different convective adjustment timescales for land and ocean in contrast to having one value globally.

Following a comparative analysis of 5-year-long climate simulations, we find τ_O = 4 hrs and τ_L = 1 hr to yield the best results. Particularly, we find better MJO simulations. Although these τ values were chosen empirically and require further tunning, the conclusion of our finding remains the same, which is the recommendation to use two different τ values for land and ocean.

1 Introduction

Deep convection is complex to parameterize [*Arakawa*, 2004]. While the explicit representation of deep convection is becoming a plausible option to navigate this "deadlock" [*Randall et al.*, 2003; *Randall*, 2013], for long-term projections of our climate, cumulus parameterization is still unavoidable. Hence, amidst the fierce emergence of convection-resolving models [*Stevens et al.*, 2019], various schemes to parameterize convection continue to develop. In particular, the recent decades have witnessed a surge of novel ideas that have accelerated this progress [*Rio et al.*, 2019, and references therein].

The “art” of tuning parameters used in convection parameterization schemes, or simply parameter tuning, plays a vital role in this development process [*Hourdin et al.*, 2017]. While deficiencies of convective parameterization are primary factors for model biases, it alone cannot alleviate all mode biases [*Goswami et al.*, 2017]. Hence, parameter sensitivity investigations are necessary not only to optimize the performance of a scheme but also to understand the extremities to which a scheme can be held responsible for biases in a simulation [*Qian et al.*, 2015; *Goswami et al.*, 2017]. In this study, we aim to contribute to understanding one tunable parameter, the convective adjustment timescale τ, by investigating the sensitivity of climate simulations to two dif-

ferent τ values for land and ocean in contrast to having one value globally in the Zhang-McFarlane convective parameterization scheme [*Zhang and McFarlane*, 1995, ZM95 hereafter] in the Community Atmospheric Model (CAM), the atmospheric model of the Community Earth System Model [*Danabasoglu et al.*, 2020].

In CAM, deep convection is represented using the Zhang-McFarlane (ZM) convection parameterization scheme. The ZM is an adjustment-type convective parameterization scheme where the atmospheric instability is removed via an adjustment towards a background state. In ZM, convective available potential energy (CAPE) defines atmospheric instability, and τ is the CAPE consumption time. In their paper, ZM95 used τ values of 2, 4, and 6 hours. To quote ZM95, "The adjustment time scale determines the intensity and duration of convection for a given CAPE. With small τ the convection is short-lived but intensity is high, on the other hand with larger τ the convection is long-lived but of low intensity". ZM95 reported their scheme to be particularly sensitive to the choice of τ. Since there is no strict range of τ, several studies investigated the sensitivity of CAM simulations to different τ values. For example, *Mishra and Srinivasan* [2010] used τ=[1,∞]. Contrasting water-vapor isotope simulations in a suite of CAM single-column simulations with a range of τ values, *Lee et al.* [2009] found their simulations to match better with satellite observations with τ = 8 hrs. *Mishra* [2011, 2012] prescribed τ = 8 hrs in global climate simulations and noted improvements in the simulations of tropical climate, especially the convectively coupled equatorial waves. Evaluating 22 tunable parameters in CAM, *Qian et al.* [2015] reported τ as one of the most critical tuning parameters. In all of the above studies, τ has a single value globally.

One value of τ globally is not a logical choice because deep convection exhibits different behaviors over continents and oceans [*Hagos et al.*, 2013; *Matsui et al.*, 2016; *Roca et al.*, 2017; *Roca and Fiolleau*, 2020]. Since the width of a thermal plume is steered by boundary layer height [*Williams and Stanfill*, 2002], a deep continental boundary layer generates wider updraft velocities in deep convection [*Lucas et al.*, 1994]. *Matsui et al.* [2016] provided a climatological view of the contrast between oceanic and continental convective precipitating clouds from long-term TRMM satellite multisensor statistics. They found large proportions of deep clouds over land. *Zipser et al.* [2006] also found the most intense storms typically over continents. These observations suggest that the atmospheric deep convection over land is wider and stronger than those over the oceans. In other words, atmospheric convection over land is shorter lived than that over ocean [*Roca et al.*, 2017]. It advocates for a shorter convection consumption time scale over land than over oceans which motivated us to address the following question: although two different

τ values incorporating land-ocean inhomogeneity are logical, is it fruit-bearing in a model-simulated climate? To answer this question, we investigate,

- response of the mean climate, and
- response of large-scale waves,

by contrasting 5-year-long climate simulations with and without incorporating land-ocean inhomogeneity via τ values.

Convective parameterization schemes, particularly adjustment-type schemes, are based on the idea that convection takes some time to stabilize the atmosphere to a background state. Essentially, this time taken is τ in the ZM scheme. Although numerically τ can have almost any value, it is decided based on a scale separation between the convective activity of the individual clouds and large-scale forcing. This concept is nicely depicted in Figure 1.1 of [*Davies*, 2008]. The graph in that figure is a function of timescales associated with convection, and consists of a turbulent initial segment indicating fluctuation of individual clouds, followed by a flat segment where these fluctuations smooth out, and finally a segment corresponding to longer time-scales that shows the evolution of the large scale forcing field itself. Conceptually, changing τ within a reasonable range (within the flat segment of Figure 1.1 of [*Davies*, 2008]) should not result in a dramatic change in the mean state of the simulated climate. We shall investigate it in detail in the first part of our results section.

Some changes that we expect in our experiments are in the simulated organization of convection. The organization of convection comes from the dynamic and thermodynamic impacts of convection on the atmosphere. Simply put, it is the memory of convection [*Davies et al.*, 2009], i.e. the fact that convection changes the large-scale properties, and can make their environment favorable or unfavorable to subsequent convection. Identifying sources of convective memory in cloud-resolving simulations, *Colin et al.* [2019] argued that the persistence of the state of convection contributes to convective memory. *Colin et al.* [2019] also suggested that convective memory and organization interact mutually. By altering τ we essentially alter memory associated with convection. Hence, we expect to see changes in convective organization. Taking a cue from *Mishra* [2011], we anticipate improved convective organization in the tropics for longer τ. However, land-ocean heterogeneity in τ is a unique feature of our experiments that we argue is essential based on heterogeneity in the behavior of convection over land and ocean. As supporting evidence, we

shall present an analysis of equatorial waves focusing on the MJO to evaluate the organization of convection in the second part of our results section.

The paper is organized as follows. A brief description of the methodology is provided in Section 2. Section 3 evaluates the response of the model to different τ values. Finally, a few concluding remarks are provided in Section 4.

2 Model and simulation details

We used the atmospheric model of the Community Earth System Model, version 2.1.3 (CESM 2.1.3) [*Danabasoglu et al.*, 2020], that is the Community Atmosphere Model, version 6 (CAM6), developed and maintained at the National Center for Atmospheric Research (NCAR), with longitude and latitude specifications 1.25°and 0.9°, respectively, and 32 vertical levels. We forced the model by HadISST1 climatological monthly mean SST data provided by the Met Office Hadley Centre [*Rayner*, 2003]. In short, we performed CESM "F2000climo" simulations. In general, these are atmospheric simulations forced by present-day climatology. All simulations are 6 years long, and we analyzed the last 5 years of each simulation since, for atmosphere-only simulations, 1-year spin-up is enough.

We performed 5 simulations. The one with out-of-the-box τ value of 1 hour globally is called the control ($CTRL$). In the next 3 simulations, we delayed the τ value over ocean (τ_O) to 2, 3 and 4 hours keeping τ over land (τ_L) 1 hour. We called these 3 simulations $EXPT_{2h}$, $EXPT_{3h}$ and $EXPT_{4h}$, respectively. We performed a last 5$^{\text{th}}$ experiment, named $EXPT_{slow}$, for which we used a τ value of 4 hours globally. Before starting our comparative analysis, we rename our first simulation as $EXPT_{fast}$, which initially we had named CTRL, for clarity and better fluency of narration of our findings. Table 1 depicts the τ values for different experiments.

Our analyses primarily show a comparison between the 5 aforementioned simulations. For some analyses we have used outgoing long-wave radiation (OLR) from NOAA (2.5°x 2.5°; daily from 01-Jun-1974 to 12-Dec-2019) [*Liebmann and Smith*, 1996] as observational benchmark.

3 Results

3.1 Mean Climate

Since about 75% of the global surface is ocean, in the simulations of the mean climate, we expect a similar model response in our experiments by delaying τ only over the oceans, as ear-

Experiment Name	τ_L	τ_O
$EXPT_{fast}$	1hr	1hr
$EXPT_{2h}$	1hr	2hr
$EXPT_{3h}$	1hr	3hr
$EXPT_{4h}$	1hr	4hr
$EXPT_{slow}$	4hr	4hr

Table 1. τ values for different experiments

lier studies did by having a larger τ globally. An evaluation of some of the mean features of simulated climate in our experiments confirm this. We find an increase in large-scale rainfall and a decrease in convective rain going from $EXPT_{fast}$ to $EXPT_{slow}$ (Fig 1 and Supplementary Fig S1). Similarly, we also notice warming in the lower levels, stronger warming in the upper levels, slight cooling in the mid-levels; moistening in the lower levels, and drying in the mid-levels (Fig 2 and Supplementary Fig S2). These features have been reported in earlier studies [for example, Fig 8 in *Mishra and Srinivasan*, 2010].

Investigating the mean features for land and ocean separately, we notice in addition, lower level (upper level) warming (cooling) is more (less) over land than over oceans (Fig 2). In the case of moisture, the letter "S" patterned vertical structure over the ocean is more curvy and squeezed down meaning lower level (middle level) moistening (drying) is stronger over oceans than over land and the respective peaks are vertically closer to the sea surface. These profiles, all together, indicate a model response to changes in τ in terms of the distribution of atmospheric convection and clouds, which impacts heating/cooling and moistening/drying of the air column (Supplementary Fig S2). Essentially these responses indicate an accumulation of convective instability in the atmosphere with delaying of convective adjustment time scale. It is attributable to more low-level warming over the continents and more low-level moistening over the oceans. More moistening near the ocean surface is relatively straightforwardly understandable, and it is a consequence of the atmosphere taking longer to convect with larger τ. To a zero-order approximation, as a result of the near-surface moisture pile-up in the oceanic regions, there is a moisture deficit in the lower levels over the continental regions (Fig 3 and Supplementary Fig S3a and S3b). Indeed it is apparent, in relative sense, in Fig 3. Although q_O does not exhibit a clear moistening signal,

159 the land drying in q_L is profound. The consequences are reflected in terms of changes in cloud
160 cover. In an overall declining tendency of cloud cover, from $EXPT_{fast}$ to $EXPT_{slow}$, over the
161 tropics high clouds decrease more steeply than low clouds. Low clouds decrease less rapidly over
162 the ocean compared to those over land (Fig 4). It should be noted that cloud categories are ob-
163 jectively defined in CESM. For example, low-level clouds are the ones below 700 hPa and high
164 clouds are between 400 and 50 hPa. Cloud covers are integrated for each model level correspond-
165 ing to respective cloud categories. In that regard, going from $EXPT_{fast}$ to $EXPT_{slow}$, low-cloud
166 cover changes (Fig 4) are consistent with relative surface moistness over land and ocean (Fig 3).

167 Taken together, the altered vertical profiles of moisture and temperature, distribution of con-
168 vective and large-scale rainfall, and associated clouds are consistent with the idea that convec-
169 tion is short-lived and stronger for smaller τ values and long-lived and weaker for longer τ value.
170 It is also evident from the solution of the CAPE equation in the ZM scheme, which can be ex-
171 pressed as $CAPE(t) = CAPE_o exp(\frac{-t}{\tau})$ in the absence of large-scale $CAPE$ generation, where
172 $CAPE_o$ is the values of $CAPE$ at $t = 0$. A larger τ in this expression means a slower decay of
173 $CAPE$. The duration of convection is essentially linked with its persistence and hence "mem-
174 ory". We discuss its impact on the simulation of the equatorial waves in the following section.

175 3.2 Simulation of MJO variance and propagation

176 Organization is a primary feature of tropical convection. It essentially means a cluster of
177 deep precipitating clouds tied together. An important question is, what brings these clouds to-
178 gether? In other words, what causes convection to organize? One idea to see the organization of
179 convection is through superpositions of convectively coupled equatorial waves (CCEWs). These
180 atmospheric waves and tropical convection are entangled. In the tropics, the atmosphere responds
181 to convective heating in terms of waves that, in turn, organize convection. Therefore, the fidelity
182 of a model in simulating tropical climate is essentially its ability to simulate the CCEWs. A stan-
183 dard metric to analyze CCEWs is the Takayabu-Wheeler-Kiladis (TWK) spectra [*Takayabu*, 1994a,b;
184 *Wheeler and Kiladis*, 1999]. Figure 5 depicts the symmetric and asymmetric TWK-spectra for
185 the observed and simulated outgoing long-wave radiation (OLR). Understandably, a striking fea-
186 ture of the TWK-spectra of observed OLR shown in Fig 5a and b is the spectral power near the
187 origin of the plots in the wavenumber range 1-5 and frequency 20-100 days, well known as the
188 MJO. The MJO is a combination of or envelope of other waves in the equatorial atmosphere. Hence,
189 the accuracy of MJO simulation is arguably a measure of the fidelity of accurate simulation of

waves in the atmosphere [*Zhang et al.*, 2020]. *Guo et al.* [2015] showed in detail that the accuracy of CCEW simulation is critical for a realistic MJO simulation.

A comprehensive review of the science of MJO is available in *Zhang et al.* [2020]. Prominent observed features of MJO suggest that they are most active in the Indo-Pacific warm pool with an eastward propagation. An interesting fact, along its path from the Indian to the Pacific Ocean, is that an MJO passes over the Indonesian maritime continent (IMC). During this passage, MJO and the prominent diurnal variabilities in the meteorology over the IMC islands interact and mutually influence each other. So much so that nearly half of the MJOs fail to propagate into the Pacific. It is critical, therefore, to represent the land-ocean heterogeneity as realistically as possible in climate models. Hence, we expect our experiments with logically defined different values of τ for land and ocean to improve simulated MJO features. Here, we shall present analyses evaluating the simulation of MJO variance and propagation. We can draw some idea of MJO simulation in different experiments from Fig 5. In Fig 5, the foremost remarkable feature is the increase in spectral power in the MJO wave number and frequency range for experiments with a longer τ. A closer visual inspection reveals that the MJO spectral power does not dramatically change from $EXPT_{2h}$ to $EXPT_{slow}$. For other waves, no one simulation is remarkably better than the rest. Fig 5 loosely suggests that overall the symmetric signal waves are improved for longer time scales, but there are no clear improvement for the antisymmetric part.

To bring out the active region of MJO we applied space-time filtering on OLR data containing the signal corresponding to wavenumbers 1-5 and a period of 20–100 days. In Fig 6 the variance of the MJO-filtered daily OLR anomalies is shown. In observations (Fig 6a), the peak variance is over the Indo-Pacific warm pool. Feeble variance peaks are noted in the eastern sides of the Pacific (off the Gulf of California) and Atlantic (around the western coast of Sierra Leone). It is consistent with the fact that although MJO is most active in the Indo-Pacific warm pool region, it has considerable influence modulating the convective activity over the eastern equatorial Pacific [*Maloney and Hartmann*, 2000a,b; *Maloney and Kiehl*, 2002] and Atlantic [*Klotzbach*, 2014]. For $EXPT_{fast}$ high variance is noted around the warm-pool region but widely spread and has multiple peaks. The strongest variance is around Northern Australia and the south-western Pacific region. The other secondary maxima are over the southern Bay of Bengal, the central equatorial Indian Ocean, and the central Pacific regions.

The simulated MJO variance strength and pattern experience some changes with changes in τ values. In general, a slower τ_O keeping τ_L same yields more variance. In other words, it in-

creases convective activity in MJO space and time scales. In $EXPT_{2h}$ a pronounced peak is located over the western-central equatorial Pacific with two secondary maxima near the south-western equatorial Pacific and eastern equatorial Indian Ocean. In $EXPT_{3h}$ the variance is more concentrated over the western equatorial Pacific, with a secondary peak south of the central equatorial Indian Ocean. With larger values of τ_L, the maximum variance gets more and more focused over the warm pool region, from $EXPT_{fast}$ to $EXPT_{3h}$ (comparing Fig 6b-d). It is noteworthy, that all the pronounced peaks for $EXPT_{2h}$ and $EXPT_{3h}$ are over oceans, in and around the Indo-Pacific warm pool region, but split unlike observations (Fig 6a). The model simulated MJO variance further slowing τ_O to 4 hours ($EXPT_{4h}$ shown in Fig 6e) suggests that MJO variance does not necessarily increase with increasing τ_O. The variance peak intensities are visibly weaker in $EXPT_{04}$ compared to that in $EXPT_{2h}$ and $EXPT_{3h}$ and more only than that in $EXPT_{fast}$. However, a noteworthy feature of $EXPT_{4h}$, a fine detail missing in all other simulations, is the variance peaks near the eastern side of the equatorial Pacific and Atlantic oceans. Baring these subtle variance peaks, $EXPT_{slow}$ looks the best, although still a considerably weaker variance peak compared to observations. The variance fields normalized by the respective domain means are available in Supplementary Fig S4, which depicts a better visual illustration of the variance peaks.

A prominent feature of MJOs is eastward propagation. The propagation features of the MJO are arguably better characterized by Hovmöller plots averaged over the latitude band between 10°S and 10°N, shown in Fig 7. Each frame in Fig 7 depicts 10°S-10°N averaged cross-correlations of OLR anomalies with MJO-index. The MJO-index is defined as the 20-100-day filtered OLR anomalies averaged over 5°S-5°N, 75°E-85°E following *Guo et al.* [2015]. It is noteworthy to mention, reiterating *Guo et al.* [2015], the philosophy behind using such an MJO index. An index based on a 20-100 day filter brings out the dominant intraseasonal signal in the data that ideally should be an MJO signal. The eastward propagating red and blue patches of correlation values in observations (Fig 7a) confirm it. We note the phase speed is faster over the west Pacific (east of ~120°E) than that over the Indian Ocean (west of ~100°E). The relatively slow phase speed in the longitude range ~100°-120°E is collocated with the Indonesian archipelago. These different phase speeds over land and oceanic regions are consistent with MJO interaction with the profound diurnal variations of meteorology over the MC. It furthermore emphasizes the need to mimic land-ocean heterogeneity realistically in climate models.

To assess the performance of our different experiments in simulating MJO propagation features, we recall the "good" and "bad" models of *Guo et al.* [2015]. In Figure 2, *Guo et al.* [2015] showed that the "good" models simulated more realistic eastward propagation than the "bad" mod-

els. In Fig 7, $EXPT_{4h}$ is the only experiment with an eastward propagation and exhibits some resemblance with observations and the only "good" model, albeit with some key caveats. The positive anomalies almost abruptly died over the MC and reappeared over the western Pacific. Nonetheless, an intriguing observation, that contains the novelty of our research, is the more realistic eastward propagation simulated in $EXPT_{4h}$ than in $EXPT_{slow}$. An improved simulation of eastward propagation in $EXPT_{4h}$ supports our argument that using two τs for land and ocean is a logical choice. It reconfirms our anticipation that representing land-ocean heterogeneity via τ in ZM in CAM alters convective memory and affects the organization of convection. A larger τ_O than τ_L, although reasonable, is only based on intuition. Detailed sensitivity analysis would be needed to investigate and pin down the best pair of τ values.

4 Discussion and Conclusion

Climate models continue to grow, fueled by a growing understanding of the earth system. Hence, it is only logical to include a fairly well-recognized and relatively old knowledge about land and ocean heterogeneity of atmospheric convection in the parameterization of convection. We argue that using two different τ in ZM in CAM can be one simple yet fruit-bearing way. In our experiments to investigate the model response to land-ocean heterogeneity in τ values, we used τ_L = 1 hr, and τ_O = 2 hrs, 3 hrs, 4 hrs. In two additional experiments, $EXPT_{fast}$ and $EXPT_{slow}$, we used $\tau_L = \tau_O$ = 1 hr and $\tau_L = \tau_O$ = 4 hrs, respectively, to complement the previous group of experiments. The τ values that we have used are informed by our knowledge of frequency, life-cycle, and behavior of atmospheric convection over land and ocean learned from previous studies [*Lucas et al.*, 1994; *Williams and Stanfill*, 2002; *Zipser et al.*, 2006; *Hagos et al.*, 2013; *Matsui et al.*, 2016; *Roca et al.*, 2017; *Roca and Fiolleau*, 2020] and inspired by results of relevant model sensitivity experiments [*Zhang and McFarlane*, 1995; *Lee et al.*, 2009; *Mishra and Srinivasan*, 2010; *Mishra*, 2011; *Misra et al.*, 2012].

Our findings regarding the model simulated mean state in different experiments are consistent with earlier studies [*Lee et al.*, 2009; *Mishra and Srinivasan*, 2010; *Mishra*, 2011; *Misra et al.*, 2012]. For example, total rainfall remained approximately the same while large-scale rainfall increased and convective rain decreased for longer τ_Ls. Consistency of the model response for a slow τ only over the oceans with slowing down τ globally is most likely a result of 75% of the global surface being ocean. However, since there is no physical barrier between the atmospheric columns over continents and oceans, having two τ values in our experiments, which essentially are prescribed to represent heterogeneity in the persistence of convection over the two different

surfaces, created a distinction between the intensities with which the model responses are felt over land and ocean. For example, the oceanic boundary layer is moister and warmer than the continental boundary layer (Fig 3). Furthermore, the mid-troposphere is drier and cooler over oceans than over the continents (Fig 2). These land-ocean heterogeneities inevitably create differences in atmospheric instabilities. These instabilities are essentially realized in the form of atmospheric convection that, by design in our experiments with slower τ, takes longer to bring the atmosphere back to a background state. It is suggestive of a longer persistence of convective instability over the ocean than that over the continents which essentially can be linked with memory of convection [*Davies et al.*, 2009; *Colin et al.*, 2019; *Hwong et al.*, 2023].

The conclusion that the model simulated better convectively coupled equatorial waves in $EXPT_{2h}$ than in $EXPT_{slow}$ is a key. We conclude this based on our finding of a better MJO simulation in $EXPT_{2h}$, consistent with improved symmetric waves. Scientists had advocated in favor of a slower τ in earlier studies [*Mishra*, 2011; *Misra et al.*, 2012]. We also noted a significant increase in MJO power for τ = 4 hrs than τ = 1 hr (comparing Fig 5b and Fig 5f). However, an evaluation of the model simulated intraseasonal zonal propagation reveals that $EXPT_{4h}$ performs considerably better than $EXPT_{slow}$. This confirms that having one τ globally is not only unphysical but also slowing down tinkering persistence of convection to improve simulation of equatorial waves, and may result in model responses that might look improved, but only superficially.

Our results, in general, serve as proof of concept that a realistic representation of convective adjustment time scale over land and ocean is a logical requirement that properly implemented shall lead to improvements in climate model simulations. In specific, we advocate at least two τ values, one for the continents and one relatively slower for the oceans in ZM in CAM. The fact that we did not perform a rigorous model sensitivity analysis [e.g., *Qian et al.*, 2015; *Lin et al.*, 2016; *Goswami et al.*, 2017] nor did we perform any cloud-resolving simulation targetting the life-cycle of atmospheric convection [*Davies et al.*, 2013; *Colin et al.*, 2019; *Daleu et al.*, 2020, e.g.,] leaves a scope as well as the requirement for future research to determine the best values of τ_L and τ_O for ZM in CAM. It will hopefully guide convection parameterization schemes, especially the adjustment types, to address land-ocean heterogeneity. Specifically, we recommend that future developments of CAM should consider prescribing different τ_L and τ_O in ZM in CAM.

5 Open Research

- Model : We used the atmospheric model of the Community Earth System Model, version 2.1.3 (CESM 2.1.3) [*Danabasoglu et al.*, 2020]
- Description of the model simulations is provided in Section 2 of the manuscript. A source file of CESM 2.1.3, zm_conv.F90, modified for our experiments is provided in `https://github.com/bidyutbg/CESM_Tau_experiment.git`.
- Data analysis software: Figures 1-5 are produced in Python and the details of the methodology is provided in the relevant sections of the text. Figure 5 is produced using script available at `https://github.com/bidyutbg/CESM_Tau_experiment/blob/main/WK_spectra_FINAL-NEW.ipynb`. Figure 6 is produced using script available at `https://github.com/bidyutbg/CESM_Tau_experiment/blob/main/CCEW_variance-compare_FINAL.ipynb`. Figure 7 is produced using script available at `https://www.ncl.ucar.edu/Applications/Scripts/mjoclivar_9.ncl`.
- Model Output Data: Data archival is underway in Zenodo. Archival will be completed soon. A sample of the data is provided as Supporting Information for review purposes.

Acknowledgments

The authors gratefully acknowledge funding from the European Research Council (ERC) under the European Union's Horizon 2020 research and innovation program (Project CLUSTER, Grant Agreement No. 805041). This research was supported by the Scientific Service Units (SSU) of ISTA through resources provided by Scientific Computing (SciComp).

References

Arakawa, A. (2004), The Cumulus Parameterization Problem: Past, Present, and Future, *Journal of Climate*, *17*(13), 2493–2525, doi:10.1175/1520-0442(2004)017<2493:RATCPP>2.0.CO;2.

Colin, M., S. Sherwood, O. Geoffroy, S. Bony, and D. Fuchs (2019), Identifying the Sources of Convective Memory in Cloud-Resolving Simulations, *Journal of the Atmospheric Sciences*, *76*(3), 947–962, doi:10.1175/JAS-D-18-0036.1.

Daleu, C. L., R. S. Plant, S. J. Woolnough, A. J. Stirling, and N. J. Harvey (2020), Memory Properties in Cloud-Resolving Simulations of the Diurnal Cycle of Deep Convection, *Journal of Advances in Modeling Earth Systems*, *12*(8), doi:10.1029/2019MS001897.

Danabasoglu, G., J. Lamarque, J. Bacmeister, D. A. Bailey, A. K. DuVivier, J. Edwards, L. K. Emmons, J. Fasullo, R. Garcia, A. Gettelman, C. Hannay, M. M. Holland, W. G. Large, P. H. Lauritzen, D. M. Lawrence, J. T. M. Lenaerts, K. Lindsay, W. H. Lipscomb, M. J. Mills, R. Neale, K. W. Oleson, B. Otto-Bliesner, A. S. Phillips, W. Sacks, S. Tilmes, L. Kampenhout, M. Vertenstein, A. Bertini, J. Dennis, C. Deser, C. Fischer, B. Fox-Kemper, J. E. Kay, D. Kinnison, P. J. Kushner, V. E. Larson, M. C. Long, S. Mickelson, J. K. Moore, E. Nienhouse, L. Polvani, P. J. Rasch, and W. G. Strand (2020), The Community Earth System Model Version 2 (CESM2), *Journal of Advances in Modeling Earth Systems*, *12*(2), doi:10.1029/2019MS001916.

Davies, L. (2008), Self-organisation of convection as a mechanism for memory, Ph.D. thesis, The University of Reading.

Davies, L., R. S. Plant, and S. H. Derbyshire (2009), A simple model of convection with memory, *Journal of Geophysical Research: Atmospheres*, *114*(D17), 17,202, doi:10.1029/2008JD011653.

Davies, L., R. S. Plant, and S. H. Derbyshire (2013), Departures from convective equilibrium with a rapidly varying surface forcing, *Quarterly Journal of the Royal Meteorological Society*, *139*(676), 1731–1746, doi:10.1002/qj.2065.

Goswami, B. B., B. Khouider, R. Phani, P. Mukhopadhyay, and A. J. Majda (2017), Implementation and calibration of a stochastic multicloud convective parameterization in the NCEP <scp>C</scp> limate <scp>F</scp> orecast <scp>S</scp> ystem (CFSv2), *Journal of Advances in Modeling Earth Systems*, *9*(3), 1721–1739, doi:10.1002/2017MS001014.10.1002/2017MS001014.

Guo, Y., D. E. Waliser, and X. Jiang (2015), A Systematic Relationship between the Representations of Convectively Coupled Equatorial Wave Activity and the Madden–Julian Oscillation in Climate Model Simulations, *Journal of Climate*, *28*(5), 1881–1904, doi:10.1175/JCLI-D-14-00485.1.10.1175/JCLI-D-14-00485.1.

Hagos, S., Z. Feng, S. Mcfarlane, and L. R. Leung (2013), Environment and the Lifetime of Tropical Deep Convection in a Cloud-Permitting Regional Model Simulation, *Journal of the Atmospheric Sciences*, *70*(8), 2409–2425, doi:10.1175/JAS-D-12-0260.1.

Hourdin, F., T. Mauritsen, A. Gettelman, J. C. Golaz, V. Balaji, Q. Duan, D. Folini, D. Ji, D. Klocke, Y. Qian, F. Rauser, C. Rio, L. Tomassini, M. Watanabe, and D. Williamson (2017), The Art and Science of Climate Model Tuning, *Bulletin of the American Meteorological Society*, *98*(3), 589–602, doi:10.1175/BAMS-D-15-00135.1.

Hwong, Y.-L., M. Colin, P. Aglas-Leitner, C. Muller, and S. Sherwood (2023), Assessing Memory in Convection Schemes Using Idealized Tests, *ESS Open Archive*, *preprint*.

Klotzbach, P. J. (2014), The Madden–Julian Oscillation's Impacts on Worldwide Tropical Cyclone Activity, *Journal of Climate*, *27*(6), 2317–2330, doi:10.1175/JCLI-D-13-00483.1.

Lee, J. E., R. Pierrehumbert, A. Swann, and B. R. Lintner (2009), Sensitivity of stable water isotopic values to convective parameterization schemes, *Geophysical Research Letters*, *36*(23), doi:10.1029/2009GL040880.

Liebmann, B., and C. Smith (1996), Description of a Complete (Interpolated) Outgoing Longwave Radiation Dataset., *Bulletin of the American Meteorological Society*, *77*, 1275–1277.

Lin, G., H. Wan, K. Zhang, Y. Qian, and S. J. Ghan (2016), Can nudging be used to quantify model sensitivities in precipitation and cloud forcing?, *Journal of Advances in Modeling Earth Systems*, *8*(3), 1073–1091, doi:10.1002/2016MS000659.

Lucas, C., E. J. Zipser, and M. A. Lemone (1994), Vertical Velocity in Oceanic Convection off Tropical Australia, *Journal of the Atmospheric Sciences*, *51*(21), 3183–3193, doi:10.1175/1520-0469(1994)051<3183:VVIOCO>2.0.CO;2.

Maloney, E. D., and D. L. Hartmann (2000a), Modulation of Eastern North Pacific Hurricanes by the Madden–Julian Oscillation, *Journal of Climate*, *13*(9), 1451–1460, doi:10.1175/1520-0442(2000)013<1451:MOENPH>2.0.CO;2.

Maloney, E. D., and D. L. Hartmann (2000b), Modulation of Hurricane Activity in the Gulf of Mexico by the Madden-Julian Oscillation, *Science*, *287*(5460), 2002–2004, doi:10.1126/science.287.5460.2002.

Maloney, E. D., and J. T. Kiehl (2002), MJO-Related SST Variations over the Tropical Eastern Pacific during Northern Hemisphere Summer, *Journal of Climate*, *15*(6), 675–689, doi:10.1175/1520-0442(2002)015<0675:MRSVOT>2.0.CO;2.

Matsui, T., J. D. Chern, W. K. Tao, S. Lang, M. Satoh, T. Hashino, and T. Kubota (2016), On the Land–Ocean Contrast of Tropical Convection and Microphysics Statistics Derived from TRMM Satellite Signals and Global Storm-Resolving Models, *Journal of Hydrometeorology*, *17*(5), 1425–1445, doi:10.1175/JHM-D-15-0111.1.

Mishra, S. K. (2011), Influence of convective adjustment time scale on the tropical transient activity, *Meteorology and Atmospheric Physics*, *114*(1), 17–34, doi:10.1007/S00703-011-0154-8/FIGURES/19.

Mishra, S. K. (2012), Effects of convective adjustment time scale on the simulation of tropical climate, *Theoretical and Applied Climatology*, *107*(1-2), 211–228, doi: 10.1007/S00704-011-0479-8/FIGURES/19.

Mishra, S. K., and J. Srinivasan (2010), Sensitivity of the simulated precipitation to changes in convective relaxation time scale, *Annales Geophysicae*, *28*(10), 1827–1846, doi: 10.5194/ANGEO-28-1827-2010.

Misra, V., P. Pantina, S. Chan, and S. DiNapoli (2012), A comparative study of the Indian summer monsoon hydroclimate and its variations in three reanalyses, *Climate Dynamics*, *39*(5), 1149–1168, doi:10.1007/s00382-012-1319-y.

Qian, Y., H. Yan, Z. Hou, G. Johannesson, S. Klein, D. Lucas, R. Neale, P. Rasch, L. Swiler, J. Tannahill, H. Wang, M. Wang, and C. Zhao (2015), Parametric sensitivity analysis of precipitation at global and local scales in the Community Atmosphere Model CAM5, *Journal of Advances in Modeling Earth Systems*, *7*(2), 382–411, doi: 10.1002/2014MS000354.

Randall, D., M. Khairoutdinov, A. Arakawa, and W. Grabowski (2003), Breaking the Cloud Parameterization Deadlock, *Bulletin of the American Meteorological Society*, *84*(11), 1547–1564, doi:10.1175/BAMS-84-11-1547.

Randall, D. A. (2013), Beyond deadlock, *Geophysical Research Letters*, *40*(22), 5970–5976, doi:10.1002/2013GL057998.

Rayner, N. A. (2003), Global analyses of sea surface temperature, sea ice, and night marine air temperature since the late nineteenth century, *Journal of Geophysical Research*, *108*(D14), doi:10.1029/2002JD002670.

Rio, C., A. D. Del Genio, and F. Hourdin (2019), Ongoing Breakthroughs in Convective Parameterization, *Current Climate Change Reports 2019 5:2*, *5*(2), 95–111, doi: 10.1007/S40641-019-00127-W.

Roca, R., and T. Fiolleau (2020), Extreme precipitation in the tropics is closely associated with long-lived convective systems, *Communications Earth & Environment 2020 1:1*, *1*(1), 1–6, doi:10.1038/s43247-020-00015-4.

Roca, R., T. Fiolleau, and D. Bouniol (2017), A Simple Model of the Life Cycle of Mesoscale Convective Systems Cloud Shield in the Tropics, *Journal of Climate*, *30*(11), 4283–4298, doi:10.1175/JCLI-D-16-0556.1.

Stevens, B., M. Satoh, L. Auger, J. Biercamp, C. S. Bretherton, X. Chen, P. Düben, F. Judt, M. Khairoutdinov, D. Klocke, C. Kodama, L. Kornblueh, S. J. Lin, P. Neumann, W. M.

Putman, N. Röber, R. Shibuya, B. Vanniere, P. L. Vidale, N. Wedi, and L. Zhou (2019), DYAMOND: the DYnamics of the Atmospheric general circulation Modeled On Non-hydrostatic Domains, *Progress in Earth and Planetary Science*, *6*(1), 1–17, doi: 10.1186/S40645-019-0304-Z/FIGURES/9.

Takayabu, Y. (1994a), Large-Scale Cloud Disturbances Associated with Equatorial Waves, *Journal of the Meteorological Society of Japan. Ser. II*, *72*(3), 433–449, doi: 10.2151/jmsj1965.72.3{_}433.

Takayabu, Y. (1994b), Large-Scale Cloud Disturbances Associated with Equatorial Waves, *Journal of the Meteorological Society of Japan. Ser. II*, *72*(3), 451–465, doi: 10.2151/jmsj1965.72.3{_}451.

Wheeler, M., and G. N. Kiladis (1999), Convectively Coupled Equatorial Waves: Analysis of Clouds and Temperature in the Wavenumber-Frequency Domain, *Journal of the Atmospheric Sciences*, *56*(3), 374–399, doi:10.1175/1520-0469(1999)056<0374:CCEWAO>2.0.CO;2.

Williams, E., and S. Stanfill (2002), The physical origin of the land-ocean contrast in lightning activity, *Comptes Rendus Physique*, *3*(10), 1277–1292, doi:10.1016/S1631-0705(02)01407-X.

Zhang, C., F. Adames, B. Khouider, B. Wang, and D. Yang (2020), Four Theories of the Madden-Julian Oscillation, *Reviews of Geophysics*, *58*(3), e2019RG000,685, doi: 10.1029/2019RG000685.

Zhang, G. J., and N. A. McFarlane (1995), Sensitivity of climate simulations to the parameterization of cumulus convection in the Canadian climate centre general circulation model, *Atmosphere-Ocean*, *33*(3), 407–446, doi:10.1080/07055900.1995.9649539.

Zipser, E. J., D. J. Cecil, C. Liu, S. W. Nesbitt, and D. P. Yorty (2006), Where are the most: Intense thunderstorms on Earth?, *Bulletin of the American Meteorological Society*, *87*(8), 1057–1071, doi:10.1175/BAMS-87-8-1057.

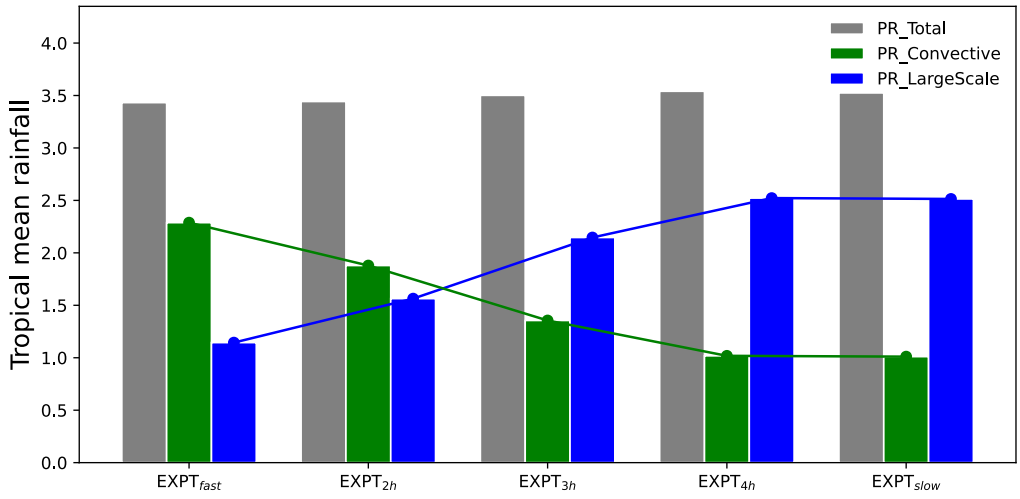

Figure 1. Tropical (tropics defined as the zonal belt between 30°S-30°N) annual mean daily rainfall (mm/day) for different experiments mentioned in Table 1.

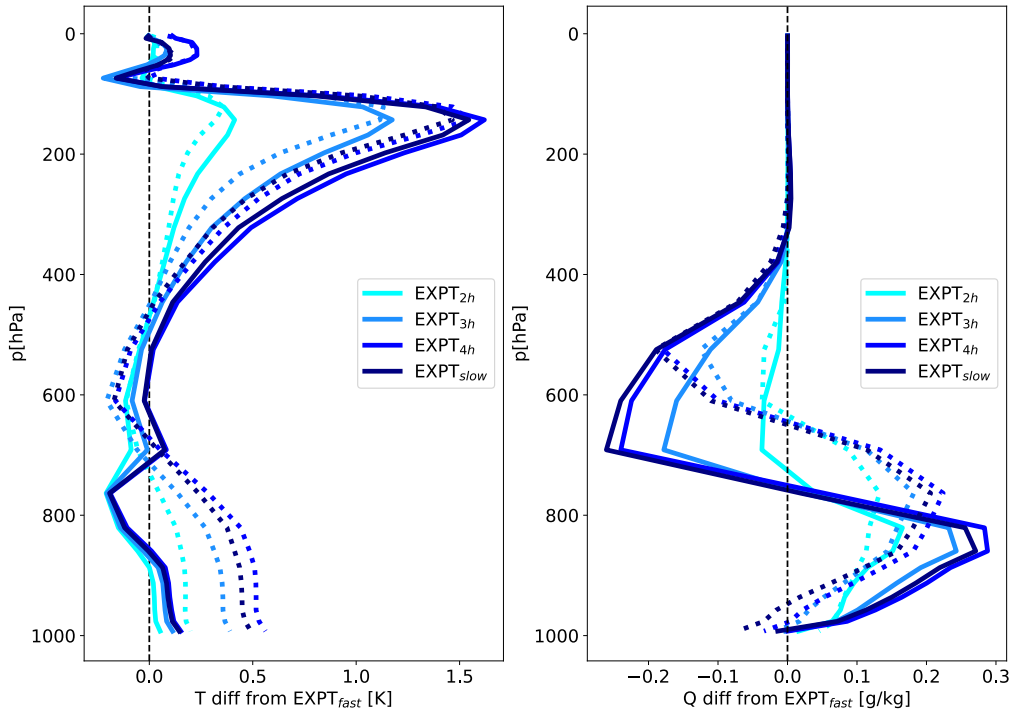

474 **Figure 2.** Tropical (tropics defined as the zonal belt between 30°S-30°N) mean vertical profiles of tem-
475 perature (T) and specific humidity (Q). Departures of different experiments, as indicated in the legends, from
476 $EXPT_{fast}$ (Land: Dotted, Ocean: Solid). The verital dashed line indicate the zero line.

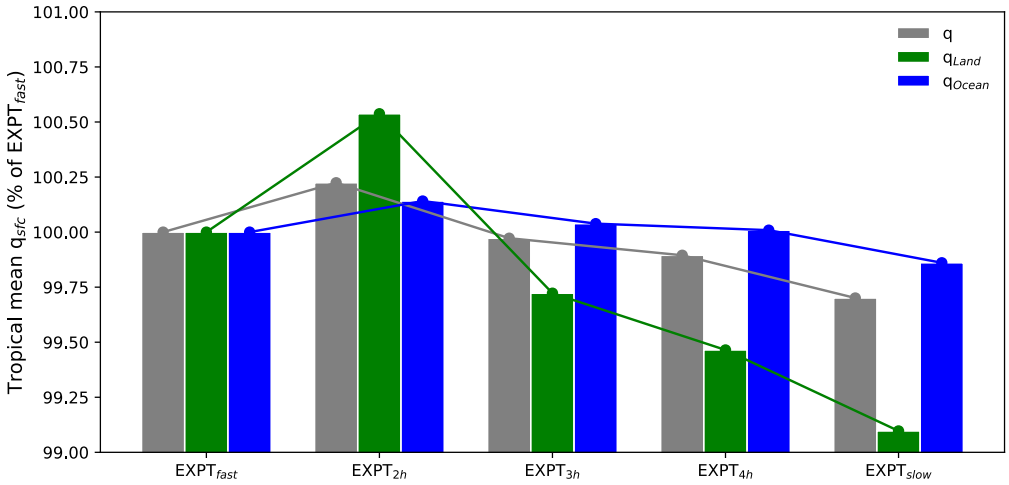

Figure 3. Tropical (tropics defined as the zonal belt between 30°S-30°N) annual daily mean specific humidity as surface depicted as % of $EXPT_{fast}$.

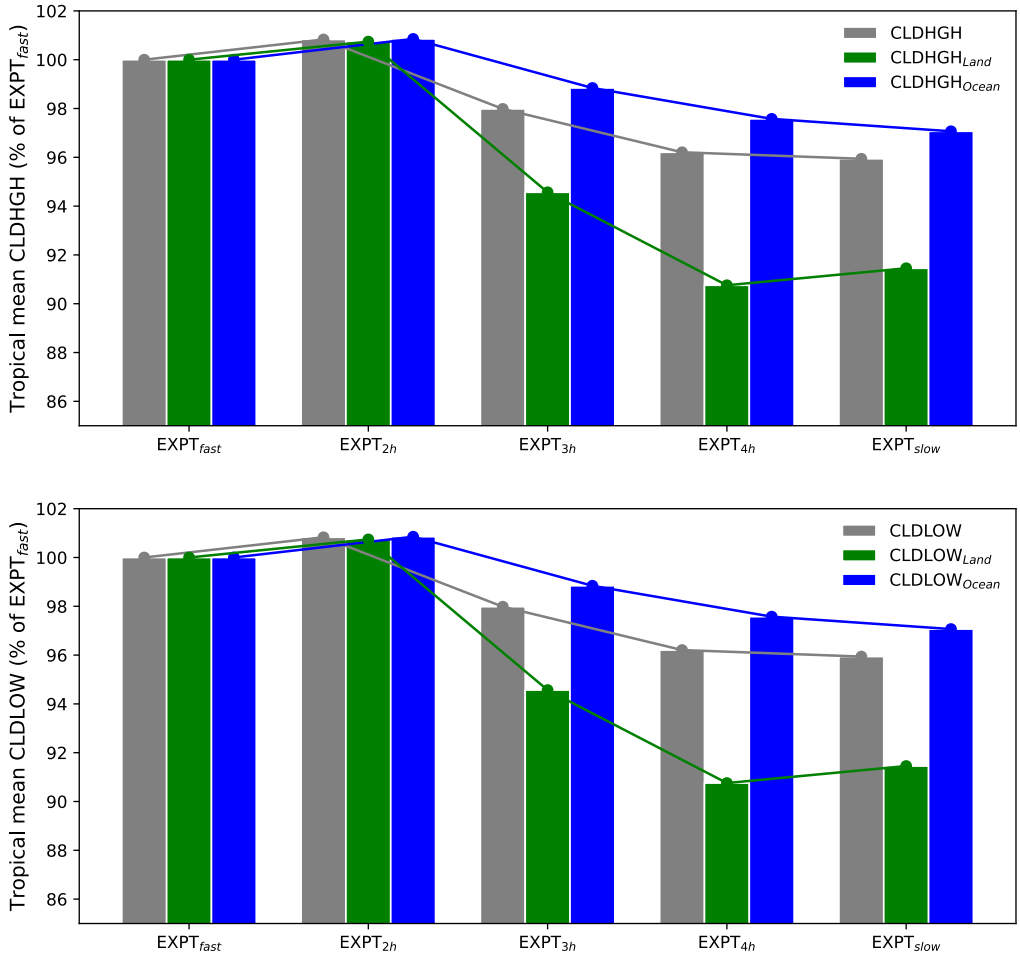

Figure 4. Tropical (tropics defined as the zonal belt between 30°S-30°N) annual daily mean High and Low cloud cover depicted as % of $EXPT_{fast}$.

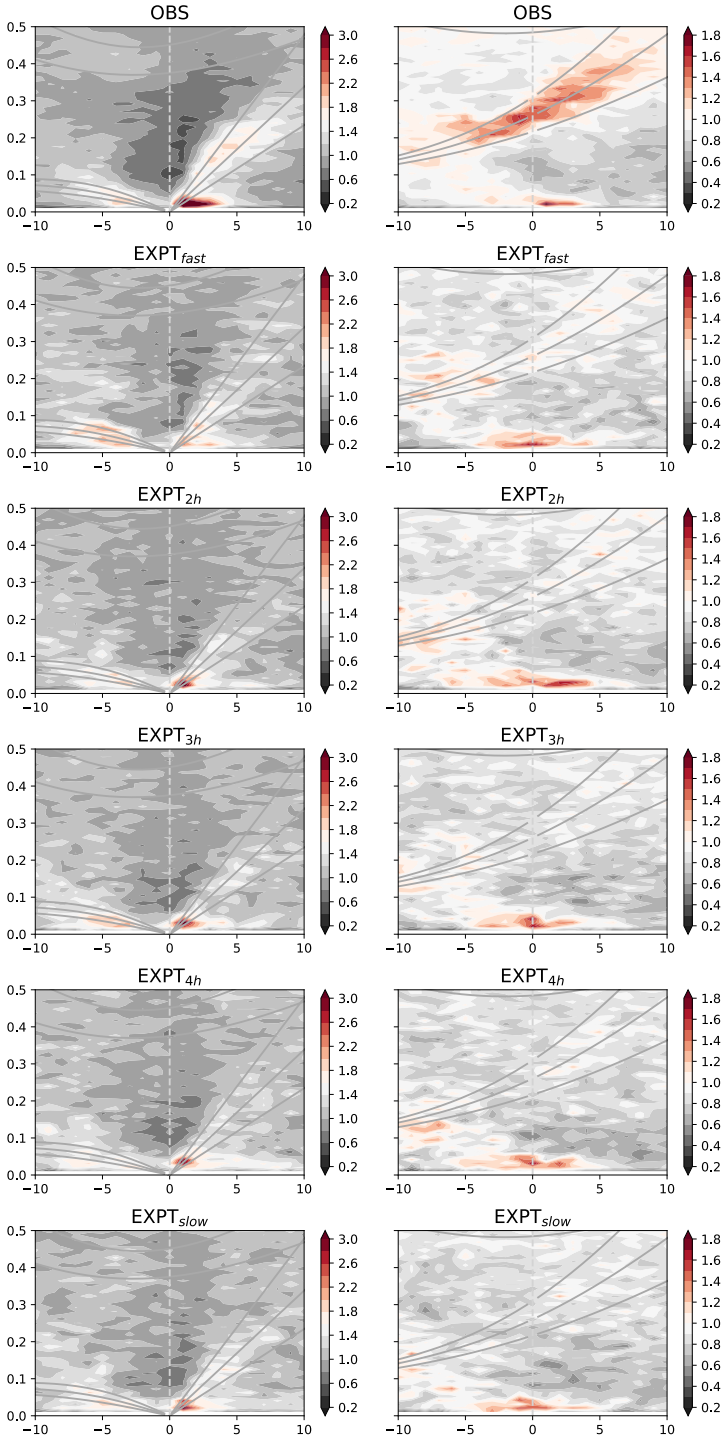

Figure 5. Takayabu-Wheeler-Kiladis spectra of OLR for OBS (from NOAA) and different experiments (as named above each panel), for the symmetric component (left-hand side panels) and antisymmetric component (right-hand side panels).

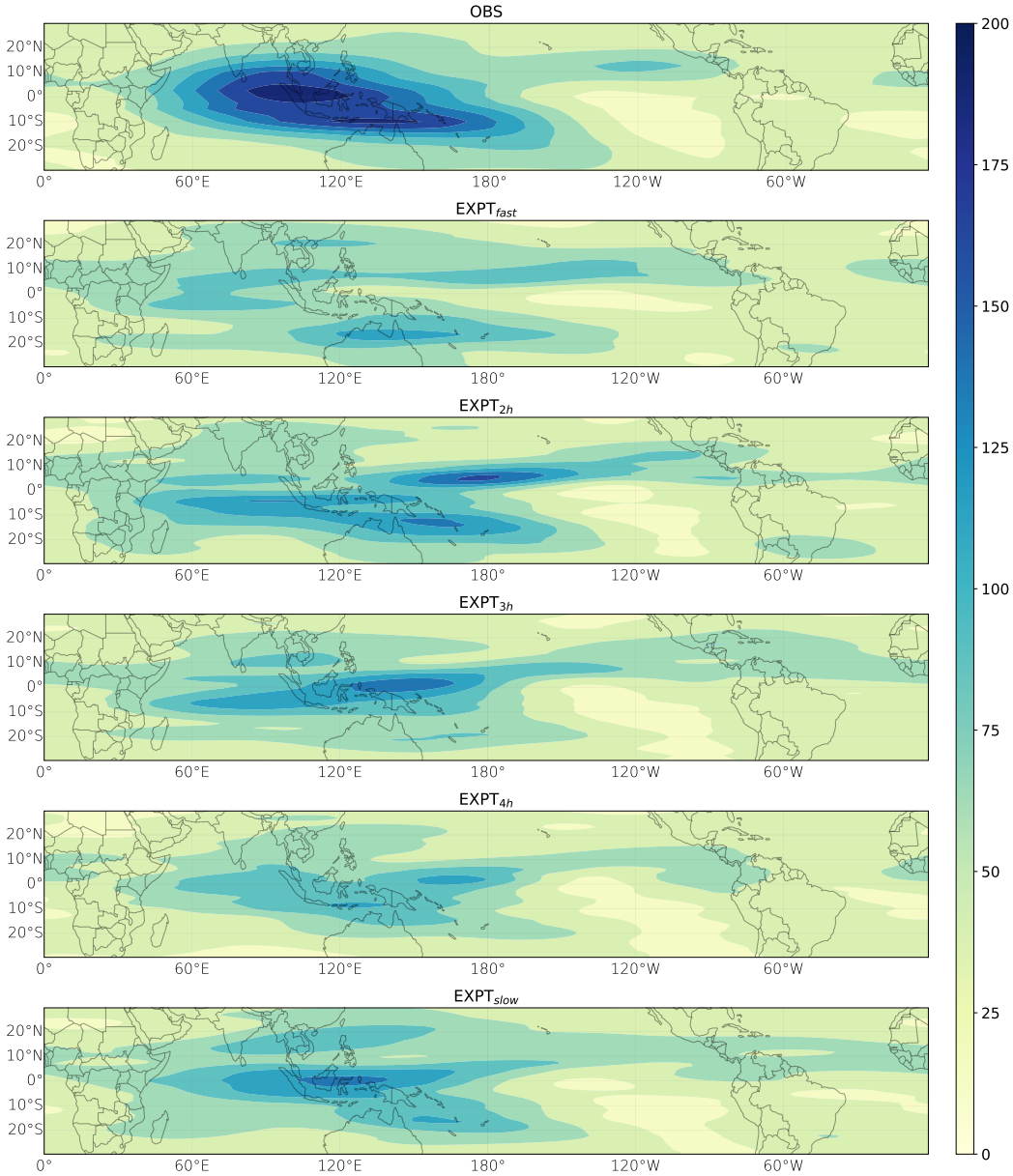

484 **Figure 6.** MJO variance computed as the daily variance of OLR data filtered for 1-5 wavenumber and 20-
485 100 day frequency, for OBS (from NOAA) and different experiments (as named above each panel).

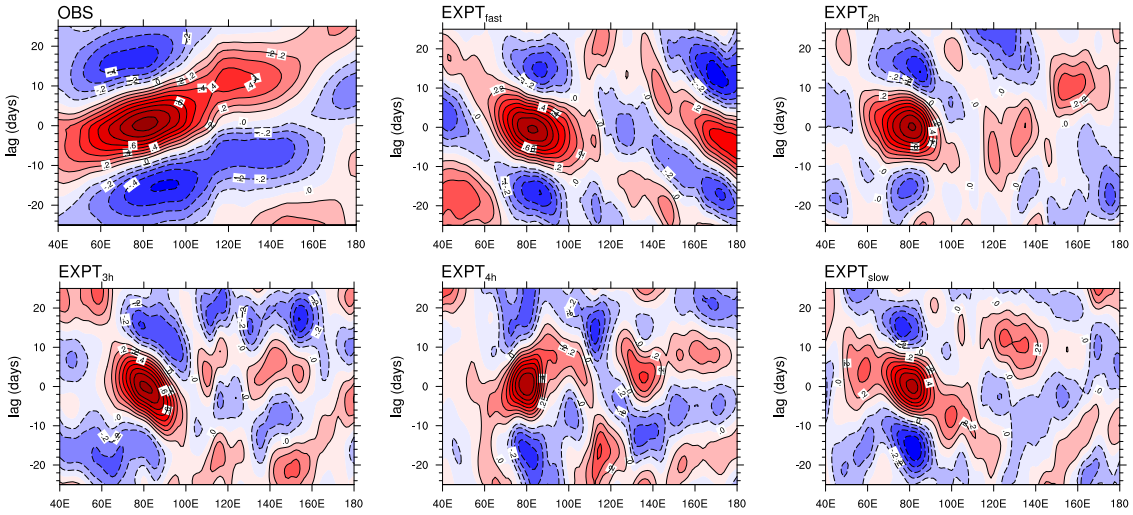

Figure 7. MJO propagation: Hovmoller (averaged from 10°S to 10°N) plots of MJO-filtered OLR (W m-2) anomalies (Winter), for OBS (from NOAA) and different experiments (as named above each panel).